Analysis of Titanium Mesh Ti6Al4V Formation Using Die Press Forming Machine for Cranioplasty

Ahmad Ayyub Syaiful Rizal[1], Mahros Darsin[1*], Robertoes Koekoeh K. Wibowo[1], Khairul Anam[2]

[1]*Department of Mechanical Engineering, Jember University, Jl. Kalimantan, Tegalboto No.37, Jember, 68121, Indonesia*
[2]*Department of Electrical Engineering, Jember University, Jl. Kalimantan, Tegalboto No.37, Jember, 68121, Indonesia*
**Corresponding author: mahros.teknik@unej.ac.id*

Article history:
Received: 27 July 2024 / Received in revised form: 22 October 2024 / Accepted: 28 October 2024
Available online 19 November 2024

ABSTRACT

Cranioplasty is required for patients with head defects, where the deformed part of the head is replaced with Ti6Al4V titanium wire implants. The titanium wire forming process is usually done manually, which can take a long time and give results that do not match the anatomical shape of the head. Therefore, it is important to develop domestic technology that can produce titanium wire automatically. This study aims to analyze the frame and mold of the automatic wire mesh molding machine before production. The tool is made using press forming method and finite element analysis with ANSYS software. The machine frame is made of 304 stainless steel material, while the mold uses ABS material. The analysis was performed with a constant load force of 100 N, corresponding to the maximum reading on the load cell. The simulation results show the deformation, strain, and von Mises stress of the machine frame and punch model, which are still far below the plastic deformation and UTS values of the material. However, the analysis results on the Ti6Al4V titanium die and mesh exceeded the UTS of the material in the cutting edge area of the die. Nevertheless, the die model can still be used because the maximum stress point is located at the edge of the die design area, where the titanium mesh will be cut when applied to the patient's skull implant. The results of this study are expected to help medical personnel in skull implant surgery and analysis of press machine manufacturing.

Keywords: *Anthropometry, cranial implant, press forming, static structural, Titanium Ti6Al4V*

I. Introduction

The head is a vulnerable part of the body because it contains vital organs such as the brain that controls the nervous system, and is protected by a skull that functions to protect from impact and form the structure of the face from the accident case does not rule out the possibility of head injuries, which can be grouped into three categories: scalp damage, skull fracture, brain injury, or a combination of the three [1].

In Indonesia, work accident data recorded more than 120,000 cases until October 2020. Of these, there were 4,275 cases of accidents with head injuries [2]. These problems require medical treatment to treat damage to the brain, skull, or scalp, prevent complications such as infection or further damage, and restore normal body function. One of the medical measures that can be taken is cranioplasty to treat bone problems in the head.

DOI: 10.17977/um016v8i22024p445

Cranioplasty is a surgical procedure performed to repair or replace missing damaged parts of the skull bone due to injury, infection, tumor, or previous surgery. Cranioplasty surgical procedures require mapping of the anatomical parts of the head called the frontal, parietal, temporal, and occipital skulls [3], [4].

Skull implant surgery uses alloplastic or non-biological materials such as polymers and metals, applied to any form of cranial defect [5]. Alloplastic materials are chosen because they have better material strength compared to human bone and are biomaterials, making them acceptable to the human body [6]. Skull implants generally use titanium Ti6Al4V in the form of wire mesh, which has high strength, is lightweight, corrosion-resistant, and has an oxide layer that can integrate with bone progenitor cells. Therefore, when the implant is applied, there is no reaction such as infection or deformation due to the impact [7], [8].

Previous research has been conducted by Neurosurgeon Adji et al. [9] on head surgery using the OTA method before surgery. Subsequent research involved performing frontal bone implant surgery using titanium Ti6Al4V wire mesh [10]. Before the implant is placed, the wire mesh, which is still in sheet form, needs to be shaped according to the patient's skull pattern. The shaping process commonly used is still a simple method that involves using medical forceps as a tool to shape the wire mesh [11]. This takes a long time and the results are less precise, resulting in a mismatch between the implant shape and the patient's skull and the risk of head infection. This requires a method to shape the wire mesh to fit the damaged skull.

There have been many methods that have been carried out by several previous studies. Nguyen et al. [12] demonstrated a technique for forming titanium Ti6Al4V wire mesh using a manual clamping method applied with a mold made from 3D printing. Furthermore, Sunderland et al. [13] showcased a simple press tool using a manual bending method to form titanium wire mesh applied to the frontal part of the skull. All these studies still use manual methods, indicating a need for domestic innovation to develop an automatic press machine. The design of an automatic press machine requires efficient and safe electrical components [14]. The machine frame design is made simple and strong for the forming process, so the finite element analysis (FEA) is needed to ensure the safety of the machine before manufacturing [15].

Overall, this research contributes to the design of an automatic die press forming machine equipped with special molding for patients with head defects. To test the strength of the machine frame and mold structure, FEA simulations were carried out using ANSYS Static Structural. The resulting simulation result approach is made for tool-making parameters so that the tool made is in accordance with the desired specifications.

II. Material and Methods

1. Material

The process of designing a machine requires several materials necessary for its construction. The selection of the right material for its function is a crucial point in this research, as it can save time and costs. The proposed materials are used as input for simulation analysis in ANSYS software. Firstly, the material for constructing the machine frame is Hollow 4x6 mm with a thickness of 1.5 mm, made of AISI 304 stainless steel, with specifications listed in Table 1 [16]. This material is chosen due to its high corrosion resistance and suitability for medical equipment [17]. Secondly, titanium mesh Ti6Al4V is selected because it is highly suitable for cranial implants, with specifications provided in

Table 2 [18], [19]. Third, the material used for the mold is acrylonitrile butadiene styrene (ABS) because this material is easily available and cheaper than ferrous metals [20], the material specifications are included in Table 3.

Table 1. Stainless steel 304 material specifications [16]

Properties	Value
Yield strength	215 MPa
Young's modulus	204 GPa
Poisson's ratio	0.29
Density	7.85 kg/m³
Ultimate tensile strength	691 MPa

Table 2. Titanium Mesh Ti6Al4V material specifications [18],[19]

Properties	Value
Yield strength (σ_γ)	896 MPa
Ultimate tensile Strength	965 MPa
Elastic modulus (E)	116 GPa
Poisson ratio	0.34

Table 3. ABS material specifications [20]

Properties	Value
Young's modulus	2,628 MPa
Poisson's ratio	0.40890
Bulk modulus	2,978.4 MPa
Density	1.03e-06 kg/mm³
Ultimate tensile strength	51.7 MPa
Tensile yield strength	49.6 MPa

Based on the material data sheet above, the ultimate tensile strength (UTS) of each material is used to obtain the material's allowable strain. By deriving the equation from the modulus of elasticity or Young's modulus, the equation is obtained as follows:

The basic elastic modulus was calculated as follows Eq. (1).

$$E = \frac{\sigma}{\varepsilon} \quad \text{.....} \quad (1)$$

Thus, the allowable strain can be determined based on Eq. (2).

$$\varepsilon_a = \frac{\sigma_a}{E} \quad \text{.....} \quad (2)$$

The allowable stress is determined based on the Eq. (3).

$$\sigma_a = \frac{\sigma_y}{SF} \quad \text{.....} \quad (3)$$

Where is,

σ_a = Material allowable stress

ε_a = Material clearance strain

σ_y = Yield strength

In material failure, the allowable stress must be below the UTS of the material. If it exceeds, the material will fail.

2. Methods

Before creating the mold design, the method used in this research involved utilizing several software tools to manage file formats and perform meshing analysis for the simulation stages.

1. MRI/CT modeling of the patient to create the mould

MRI/CT samples of patient data obtained for samples have DCOM format which is still in the form of 2D projections, with the help of Software Slicer 5.0.3 MRI/CT data can be processed into 3D projections [21]. The flowchart of the data collection process is shown in Figure 1. This stage aims to obtain the dimensions of the human head bone which will be used as the initial mold design.

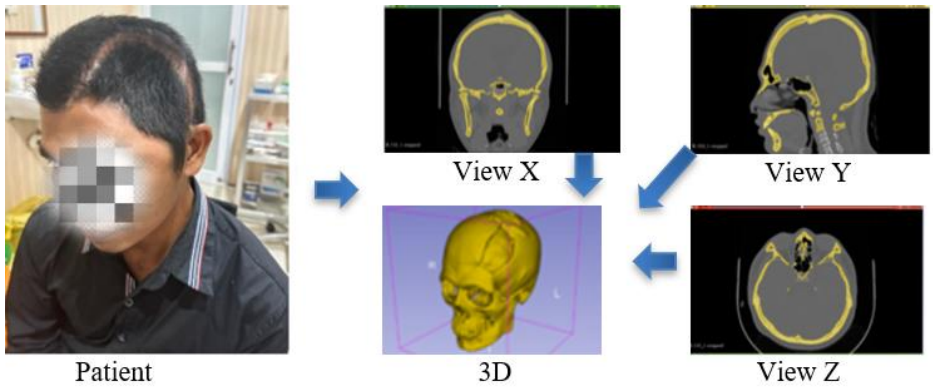

Fig. 1. Conversion of DCOM File to 3D STL

Implant reconstruction was carried out using Meshmixer software to create the mold model. This software is very user-friendly and offers many features that support complex head models [22]. In this case, Figure 2 illustrates the layout scheme of the master molding method. First, the 3D projected head model will be analyzed for any defective holes that need to be patched. Second, using the mirror method on the undamaged part of the head, a perfect head shape is created. The mirrored result is then adjusted to fit the shape of the defective head hole, resulting in an implant that closely matches the patient's head anatomy before surgery. This reconstructed result is used as the mold model for the die press forming machine.

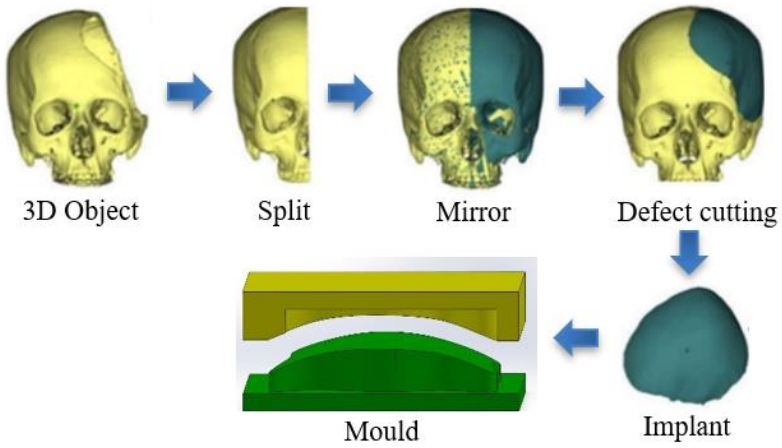

Fig. 2. Modeling the implant as a mould

2. Meshing

Meshing is an integral part of the computer-aided simulation process, the meshing process is carried out using Static Structural in ANSYS Workbench 2024 Student Software. In the simulation process, meshing has a significant influence on accuracy, convergence, and simulation speed. Size determination will be influenced by global measurement functions such as flat and curved shapes, therefore this process is very concerned in this study in order to get maximum results [23].

Analysis of meshing studies usually uses three different mesh size variations to find meshing convergence in this study [24]. The analysis of the meshing study on the machine frame was carried out using several continuous mesh size variations of 13 mm, 12 mm, 11 mm, 10 mm, and 9.5 mm as shown in Table 4. This aims to find a mesh that converges at the node size limit of 128,000 provided by ANSYS RI Student software. The results of the meshing study on the frame can be concluded that the maximum mesh size is 9.5 mm with 126,660 nodes. Based on the results of the analysis of meshing variations, there is no significant change in the results of deformation, strain, and stress. So this meshing is said to have converged for simulations performed on the machine frame simulation.

Table 4. Study of meshing on the frame

No.	Mesh element size (mm)	Nodes	Elements	Deformation max (mm)	Strain max (mm)	Stress max (MPa)
1	13	73,225	37,531	0.036280	0.000100	11.580
2	12	85,124	43,574	0.037661	0.000108	12.786
3	11	99,330	50,807	0.039131	0.000091	13.386
4	10	115,210	58,752	0.040549	0.000097	14.676
5	9.5	126,660	64,393	0.040742	0.000109	15.513

The meshing study analysis on Ti6Al4V titanium wire mesh was carried out using several continuous mesh size variations of 6 mm, 5 mm, 4 mm, 3 mm, and 2 mm, as shown in Table 5. The results of the meshing study on the titaniumTi6Al4V mesh can be concluded that the maximum mesh size is 2 mm with 87,735 nodes. Based on the results analysis of meshing variations, there is no significant change in the results of deformation, strain, and

stress. So that this meshing is said to have converged for simulations performed on the Ti6Al4V titanium wire mesh simulation.

Table 5. Study meshing on titaniumTi6Al4V mesh

No.	Mesh element size (mm)	Nodes	Elements	Deformation max (mm)	Strain max (mm)	Stress max (MPa)
1	6	79,882	27,788	10.130	0.0493	996.43
2	5	80,199	28,867	10.814	0.0591	986.52
3	4	81,892	29,974	11.021	0.0578	983.70
4	3	82,315	30,125	11.185	0.0550	979.92
5	2	87,735	32,052	11.211	0.0507	978.19

The results obtained from the meshing plot study can be seen in Figure 3(a). Meshing modeling on the punch and die was performed using a body sizing of 9.5 mm on the surface of the mold in direct contact with the titanium mesh. Meshing modeling on the Ti6Al4V titanium mesh was performed using a body sizing of 2 mm, the meshing results can be seen in Figure 3(b).

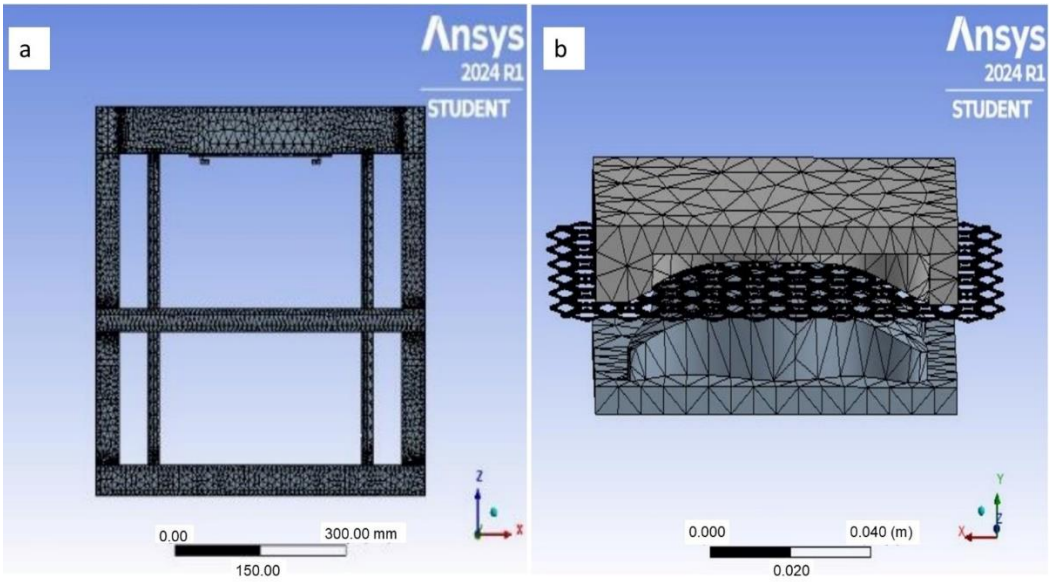

(a) (b)

Fig. 3. Meshing (a) Frame, (b) Mold and titanium mesh

III. Results and Discussions

1. Machine Design

Design concepts are needed to determine the basic, functional dimensions in the creation of an automatic die press forming machine. The machine's mechanism is made using a 1,000 kg capacity hydraulic electric jack, monitored with an Arduino Uno controller and a 100 kg capacity load cell, as shown in Figure 4. The design concept also considers ease of use so that it can be utilized by everyone, especially medical professionals.

The mold design is kept simple to save time in the 3D printing process and the assembly process on the die press forming machine. Figure 5 shows the design of the punch and die

that will be analyzed for forming titanium Ti6Al4V. The molding dimensions are based on the patient's skull defects, and the dimensions of the titanium mesh Ti6Al4V plate are 0.5 mm thick, 14 mm long, and 10 mm wide.

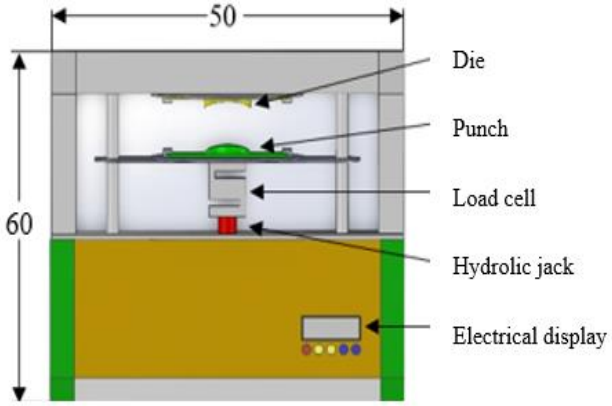

Fig. 4. Die press forming machine.

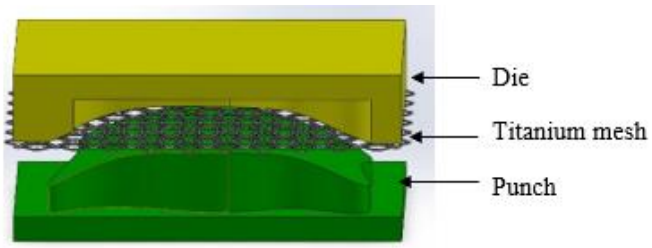

Fig. 5. Mould model

2. Static Structural Analysis

Simulation is conducted to determine the structural changes in the material that occur during die press forming and in Titanium Ti6Al4V mesh. This analysis is performed with several step settings adjusted to match the actual operating conditions of the machine. The force applied to the frame and mold is set to the maximum strength of the load cell, which is 1,000 N.

A. Deformation

The simulation process is carried out in two stages, namely frame and mold analysis, which aims to determine the maximum deformation results in the wire mesh forming process using a die-forming press machine. The analysis of the machine frame is shown in Figure 6 which shows the results of structural static deformation analysis on the machine frame of the die forming press, with the deformation range ranging from 0 mm (Min) to 0.047444 mm (Max), as indicated by the color scale on the left side. The maximum deformation occurs in the red-colored area, just below the top of the frame, with a deformation value of 0.047444 mm, while the blue-colored area, especially at the bottom of the frame, shows minimum or even zero deformation. This indicates that the greatest stress from the die-forming process occurs at the top of the frame, which receives the direct force from the forming process, while the bottom of the frame has almost no deformation. In addition, this deformation result when compared to the maximum deflection in the material data is still far below the plastic deformation value. This force distribution shows that the design of the machine frame is able to handle the force effectively, although the largest deformation is concentrated at the top,

which is a critical area to strengthen in ensuring the stability and durability of the frame during material forming operations.

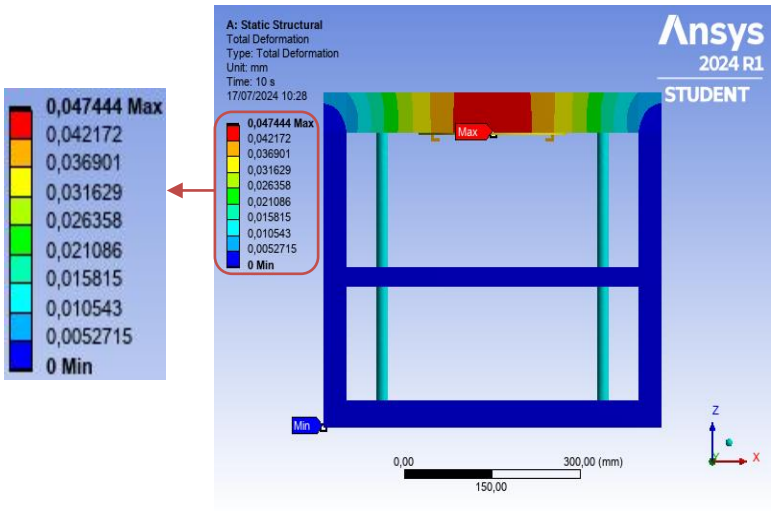

Fig. 6. Frame deformation

Figure 7 shows the results of simulating the deformation of titanium wire mesh through the finite element method (FEM) in pressure analysis using a die-forming press. In Figure 7(a), the die simulation results show the deformation distribution of the titanium wire mesh in the range of 0.0031693 mm to 0.25001 mm, with the maximum deformation occurring at the center and the minimum deformation at the edges. The pressure of the die press causes uneven deformation, where the center deforms most significantly, while the edges deform minimally. In Figure 7(b), the punch simulation results show the wire mesh deformation distribution with a range of 9.7329 mm to 11.22 mm. The maximum deformation occurs at the right bottom edge, with smaller deformations in other areas, especially in the center where it is more uniform. Figure 7(c) shows the deformation scale from 0.77154 mm to 7.267 mm, where the center of the wire mesh receives the greatest stress, causing the most deformation, while the edges undergo smaller deformations. The curved shape of the wire mesh reflects the stronger compressive force distribution at the center. This analysis emphasizes the importance of paying attention to the area of maximum deformation as a critical point in the design and forming process, as uneven pressure distribution can lead to potential material failure. The dimensional scale shows that the deformation occurs in a 40 mm long space, providing an important overview.

The results of the deformation obtained from the simulation process are then processed using graphs, as shown in Figure 8. The red graph indicates the deformation movement on the punch that occurs in the center due to its concave curve shape. The green graph represents the deformation movement from the die, with maximum results occurring at the bottom layer of the mold because the die model, resembling a convex curve, has a greater solid volume. The blue graph shows the deformation movement of the titanium mesh, with the maximum results occurring at the center position.

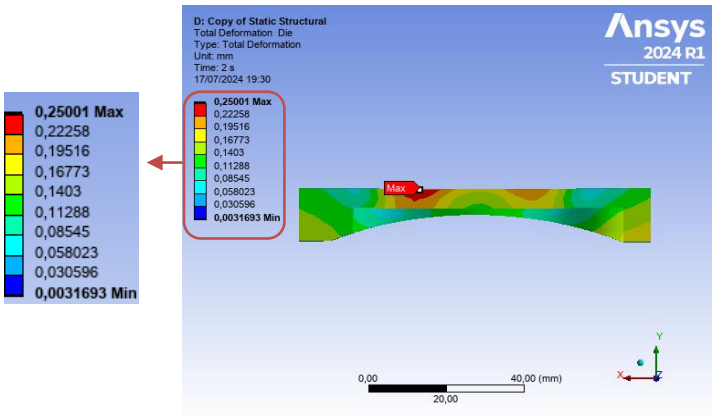

(a)

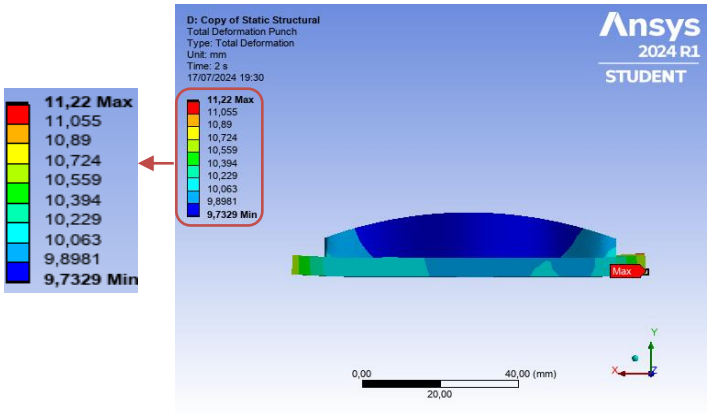

(b)

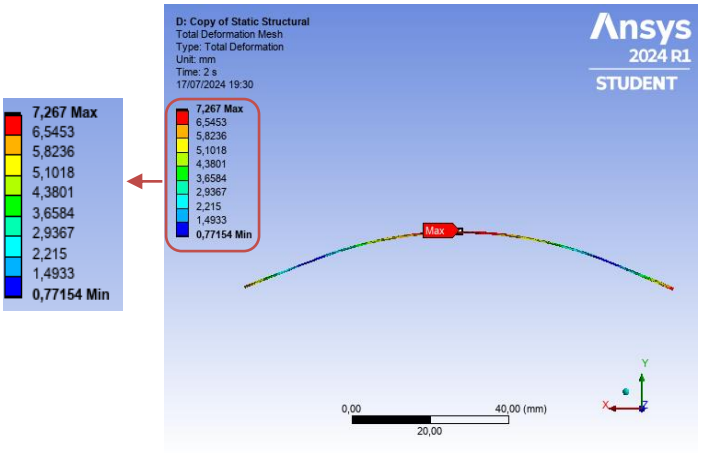

(c)

Fig. 7. Deformation results (a) Die, (b) Punch, (c) Mesh titanium

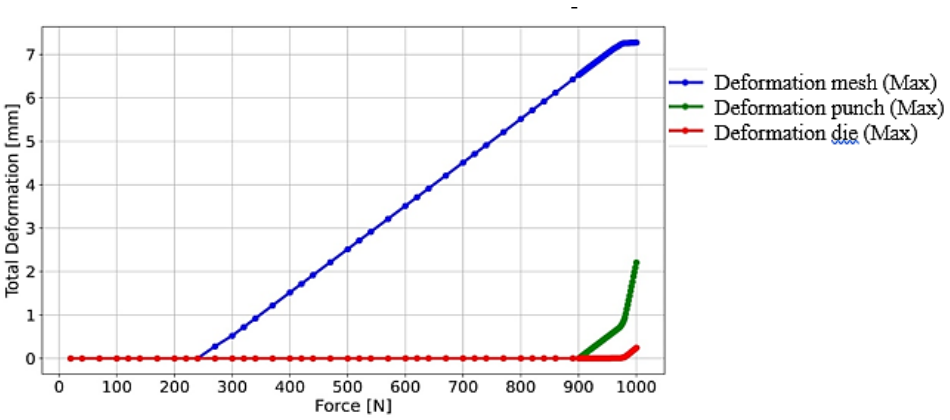

Fig. 8. Plot the maximum deformation graph

B. Strain

Strain and deformation have a relationship with the changes in the shape of an object [25]. Based on the simulation results of applying load during the wire mesh formation process using the die press forming machine, it is shown that the frame does not experience failure as illustrated in Figure 9. The simulation results indicate that the largest strain occurs at the part of the slider connected to the lower frame, measuring 0.00013396 mm. This means that the strain produced is still below 1%, and the frame undergoes elastic deformation [26].

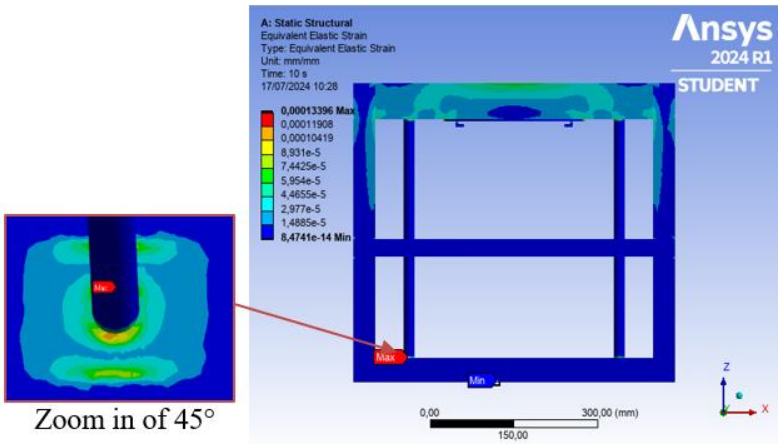

Fig. 9. Frame deformation

The results of the simulation for the titanium mesh formation process can be seen in Figure 10(a), which shows the maximum strain on the punch as 0.063243 mm, the maximum strain on the die as 0.01146 mm, and the maximum strain on the titanium mesh as 0.0098 mm, as shown in Figure 10b. It can be concluded that the strain produced is still below 1%, and the mold experiences elastic deformation.

According to Hooke's Law, deformation and strain are considered safe when they do not exceed the stress results from the simulation [27]. Figure 11 shows graphs for the mold and titanium mesh that form a linear line with the maximum strain not exceeding the stress value in the simulation. Thus, it can be concluded that the strain produced is still below 1% and the titanium mesh undergoes elastic deformation.

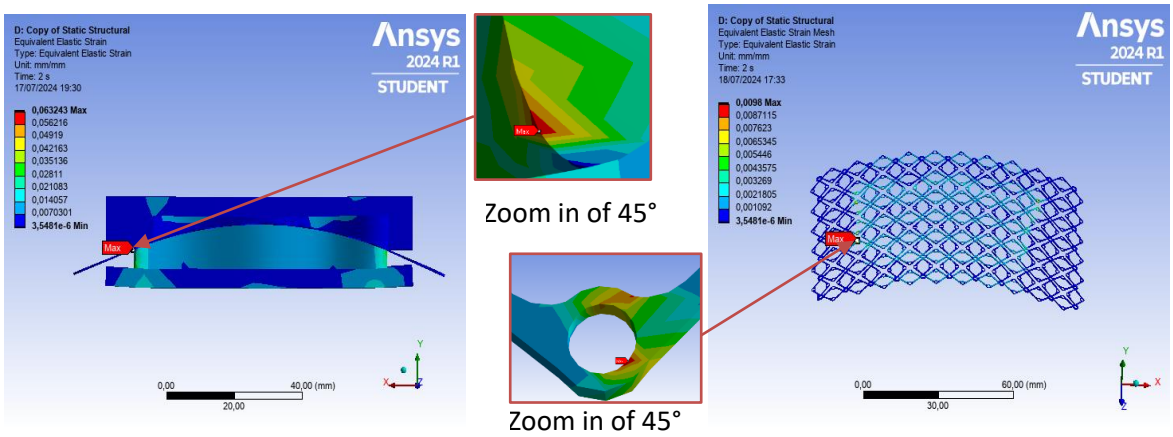

(a) (b)

Fig. 10. Strain results (a) Die and Punch, (b) Titanium mesh

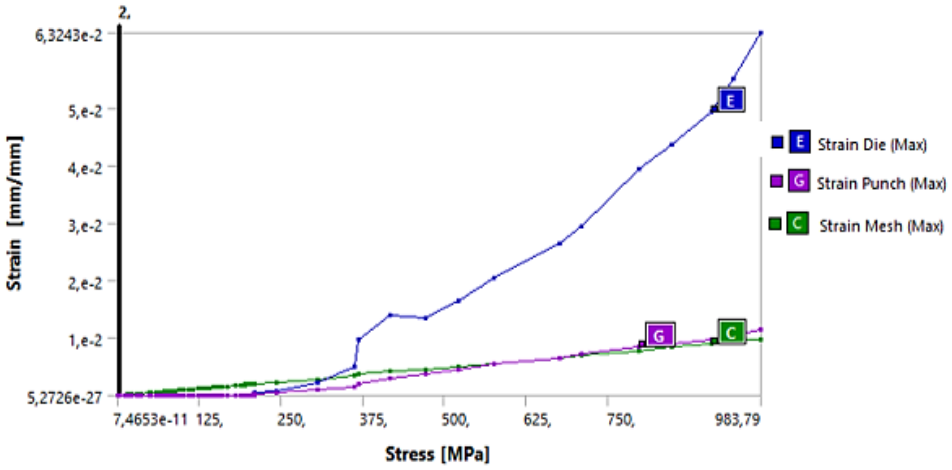

Fig. 11. Stress vs strain graph

C. Stres von-Misses

Based on Mohr's theory, the response of brittle materials to shear and normal stresses can be observed by comparing the maximum stress with the UTS and the minimum stress with the Ultimate Compressive Strength (UCS) [28], [29]. A Von Mises stress simulation analysis was conducted to determine the fatigue occurring in the material used during the wire mesh forming process with the die press forming machine. Figure 12 shows the equivalent stress in the frame, which is 25.6 MPa. The maximum stress occurs at the junction between the slider and the lower frame. It can be concluded that the stress in the frame is still below the material's UTS specification of 691 MPa.

Figure 12 shows the equivalent stress (von Mises) distribution on the die press forming machine frame with the stress scale ranging from 7.674e^{-9} MPa (minimum) to 25.62 MPa (maximum). The red contour marks the highest stress area with an equivalent stress value of 25.6 MPa that occurs at the joint between the slider and the lower frame, indicating that this area receives the most force during press operation. However, the maximum stress on the frame is still below the UTS of material strength value of 691 MPa.

The blue and green sections show areas of lower stress, where the frame is less stressed. This analysis shows that the highest stress concentrations are in critical areas of potential material failure, requiring special attention in design and materials to ensure the structural

strength and long-term durability of the frame. The even distribution of stresses in other areas indicates that the frame is quite stable, except at the points identified as having high stresses.

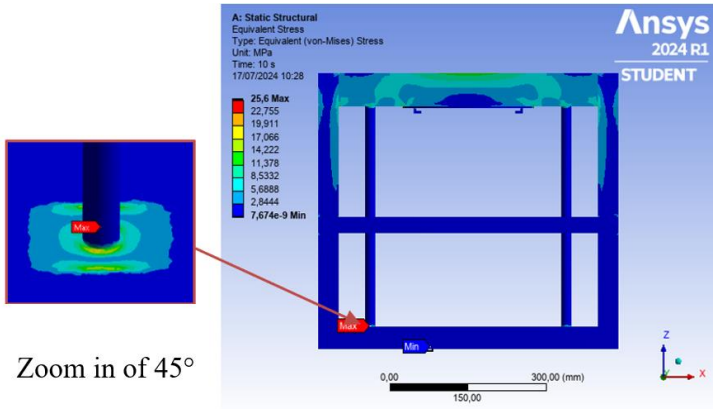

Fig 12. Results of equivalent stress frame analysis.

Simulation analysis of equivalent stress in the titanium mesh forming process is shown in Figure 13(a), with the results of the maximum stress that occurs in the punch of 14.511 MPa. Figure 13(b) shows the maximum location that occurs on the forming die is at the end of the model of 97.745 MPa. It can be concluded that the stress that occurs on the die exceeds the UTS of the ABS material which is 51.7 MPa. This is due to the design of the model used having a sharp tip, so it is necessary to add fillets at the end of the model to reduce stress results.

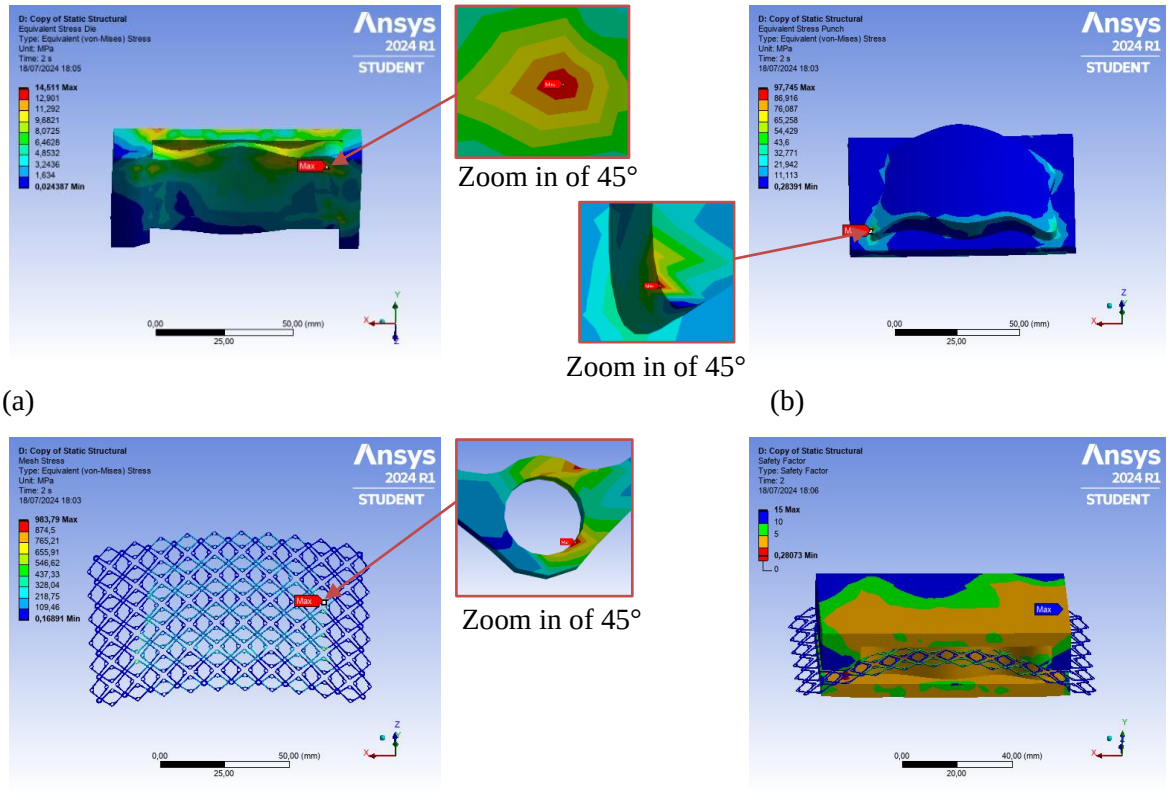

Fig 13. Equivalent stress results (a) Die, (b) Punch, (c) Mesh titanium, (d) Safety factor

The result of stress occurring on the titanium mesh occurs at the part in contact with the punch tip of 983.79 MPa as shown in Figure 13(c). This shows that the 1000 N force applied to the simulation results in the maximum stress on the titanium mesh exceeding the UTS limit, which is 965 MPa. It can be concluded that the recommended maximal force limit should be below 949.3 N.

The simulation results are used to validate the safety factor under every dynamic gait motion. The safety factor (η) should not be less than 1, and if it exceeds 15, it can be considered wasteful [30]. Figure 13 (d) shows a maximum safety factor of 15 and a minimum of 0.28073. This indicates that the simulation results show that the applied force exceeds the UTS of the titanium mesh, particularly in all the sharp-edged areas of the die mold. However, the areas of the titanium mesh experiencing UTS will be cut according to the die boundaries. Additionally, the mold in this study is designed for single use only, specifically for patients with cranial defects.

IV. Conclusions

Based on the parameter analysis of the simulation results of deformation, strain, and von-misses stress on the machine frame and punch model when compared with material data is still far below the plastic deformation value and ultimate tensile strength. While the results of the analysis of die formation and Ti6Al4V titanium mesh exceed the UTS of the material that occurs at the end of the tapered die area so that modifications such as adding fillets to the design are needed to reduce excessive stress in that area, but this die model can still be used because the maximum stress point is at the end of the die design area where the titanium mesh will be cut at that point when applied to replace the patient's cranial implant. The results of this study are expected to help medical professionals to form titanium wire mesh that fits the anatomy of the head in cranial implant cases.

References

[1] A. Tito, S.G.R. Saragih, and D. Natalia, "Comparison of revised trauma score based on intracranial haemorrhage volume among head injury patients," *Prague Med Rep*, vol. 119, no. 1, pp. 52–60, 2018, doi: 10.14712/23362936.2018.5.

[2] Ketenagakerjaan BPJS, "BPJAMSOSTEK Sudah Tangani 129.305 Kasus Kecelakaan Kerja di Indonesia.2020. (accessed Apr. 05, 2021)", https://kalbaronline.com/2020/11/26/bpjamsostek-sudah-tangani-129-305-kasus-kecelakaan-kerja-di-indonesia/

[3] L. M. Ribeiro, N. Bhindi, C. Fox, and A. Ramakrishnan, "Cranioplasty is not required in the reconstruction of small combined scalp and calvarial defects," *Journal of Plastic, Reconstructive & Aesthetic Surgery*, vol. 93, pp. 18–23, Jun. 2024, doi: 10.1016/j.bjps.2024.03.009.

[4] A. Früh, A. Zdunczyk, S. Wolf, R. Mertens, P. Spindler, D. Wasilewski et al, "Craniectomy size and decompression of the temporal base using the altered posterior question-mark incision for decompressive hemicraniectomy," Sci Rep, vol. 13, no. 1, p. 11419, Jul. 2023, doi: 10.1038/s41598-023-37689-7

[5] M.I. Martínez-Valencia, C.H. Navarro, J.A. Vázquez-López, J.L. Hernández-Arellano, J. A. Jiménez-García, and J. L. Díaz-León, "Optimization of titanium cranial implant designs using generalized reduced gradient method, analysis of finite elements, and artificial neural networks," *SCIPEDIA*, vol. 38, no. 2, pp. 1–16, 2022, doi: 10.23967/j.rimni.2022.06.004.

[6] M. Darsin, M.K. Rifky, M. Asrofi, H.A. Basuki, R.K.K.Wibowo, D. Djumhariyanto, and M.A. Choiron, "The effect of 3D printing parameter variations on tensile strength using filament made of PLA-Titanium," 2024, p. 040001. doi: 10.1063/5.0193746

[7] M.E. Ulmeanu, I.M. Mateș, C.V. Doicin, M. Mitrică, V.A. Chirteș, G. Ciobotaru, and A. Semenescu, "Bespoke implants for cranial reconstructions: Preoperative to postoperative surgery management system," *Bioengineering*, vol. 10, no. 5, May 2023, doi: 10.3390/bioengineering10050544.

[8] N. Tamburini, W. Grossi, S. Sanna, A. Campisi, F.Londero, P. Maniscalco et al, "Chest wall reconstruction using a new titanium mesh: a multicenters experience," *J Thorac Dis*, vol. 11, no. 8, pp. 3459–3466, Aug. 2019, doi: 10.21037/jtd.2019.07.74.

[9] N.K. Adji, W.Y. Putri, and M.Y. Nugraha, "Sinonasal bone destruction caused by frontal meningioma invasion related to respiratory tract infection incident: A case report," *Indonesian Journal of Neurosurgery*, vol. 5, no. 3, pp. 95-99, Sep. 2022, doi: 10.15562/ijn.v5i3.226.

[10] N.K. Adji, A.R.S. Rozidi, and R.S. Zharfan, "Removal of pineal region teratomas using occipital transtentorial approach (OTA) technique: Case report and literature review," *Int J Surg Case Rep*, vol. 76, no. 37, pp. 351–356, 2020, doi: 10.1016/j.ijscr.2020.09.174.

[11] M. Kinsman, Z. Aljuboori, T. Ball, H. Nauta, and M. Boakye, "Rapid high-fidelity contour shaping of titanium mesh implants for cranioplasty defects using patient-specific molds created with low-cost 3D printing: A case series," *Surg Neurol Int*, vol. 11, p. 288, Sep. 2020, doi: 10.25259/SNI_482_2020.

[12] B. Nguyen, O. Ashraf, R. Richards, H. Tra, and T. Huynh, "Cranioplasty using customized 3-dimensional–printed titanium implants: An international collaboration effort to improve neurosurgical care," *World Neurosurg*, vol. 149, pp. 174–180, May 2021, doi: 10.1016/j.wneu.2021.02.104.

[13] I. Sunderland, G. Edwards, J. Mainprize, and O. Antonyshyn, "A technique for intraoperative creation of patient-specific titanium mesh implants," *Plast Surg (Oakv)*, vol. 23, no. 2, pp. 95-99, 2015, doi: 10.4172/plastic-surgery.1000909.

[14] M. Gao, X. Li, H. Huang, Z. Liu, L. Li, and D. Zhou, "Energy-saving methods for hydraulic presses based on energy dissipation analysis," *Procedia CIRP*, vol. 48, pp. 331–335, 2016, doi: 10.1016/j.procir.2016.03.090.

[15] G.M. Mudennavar, G. Chalageri, and P.A. Patil, "Design and analysis of 12 ton hydraulic pressing machine," *International Journal of Scientific Development and Research*, vol. 3, 2018, [Online]. Available: www.ijsdr.org

[16] J. Liu, Z. Lv, Y. Liu, and L. Li, "Deformation behaviors of four-layered U-shaped metallic bellows in hydroforming," *Chinese Journal of Aeronautics*, vol. 33, no. 12, pp. 3479–3494, Dec. 2020, doi: 10.1016/j.cja.2020.02.007.

[17] Y. Xu, Y. Li, T. Chen, C. Dong, K. Zhang, and X. Bao, "A short review of medical-grade stainless steel: Corrosion resistance and novel techniques," *Journal of Materials Research and Technology*, vol. 29, pp. 2788–2798, Mar. 2024, doi: 10.1016/j.jmrt.2024.01.240.

[18] S. Cavalu, I.V. Antoniac, A. Mohan, F. Bodog, C. Doicin, I. Mates et al, "Nanoparticles and nanostructured surface fabrication for innovative cranial and maxillofacial surgery," *Materials*, vol. 13, no. 23, p. 5391, Nov. 2020, doi: 10.3390/ma13235391.

[19] D. Lubis, L. Indrasepta, R. Bintara, R. Ramadhan, and A. Darmawan, "The effect of thickness and type of material on the sheared edge characteristics of keychain cranioplasty plate blanking product using eccentric press machine," *Journal of*

Mechanical Engineering Science and Technology, vol. 5, no. 1, pp. 29–35, Jul. 2021, doi: 10.17977/um016v5i12021p029.

[20] K. Özsoy, A. Erçetin, and Z.A. Çevik, "Comparison of mechanical properties of PLA and ABS based structures produced by fused deposition modelling additive manufacturing," *European Journal of Science and Technology*, Nov. 2021, doi: 10.31590/ejosat.983317.

[21] K. Moiduddin, S.H. Mian, U. Umer, and H. Alkhalefah, "Fabrication and analysis of a Ti6Al4V implant for cranial restoration," *Applied Sciences (Switzerland)*, vol. 9, no. 12, Jun. 2019, doi: 10.3390/app9122513.

[22] S.H. Mian, K. Moiduddin, B.M.A. Abdo, A. Sayeed, and H. Alkhalefah, "Modelling and evaluation of meshed implant for cranial reconstruction," *The International Journal of Advanced Manufacturing Technology*, vol. 118, no. 5–6, pp. 1967–1985, Jan. 2022, doi: 10.1007/s00170-021-08161-5.

[23] K. Moiduddin, "Microstructure and mechanical properties of porous titanium structures fabricated by electron beam melting for cranial implants," Feb. 01, 2018, *SAGE Publications Ltd*. doi: 10.1177/0954411917751558.

[24] D. Sheng, R. Ma, and C. Su, "Static and modal analysis of a box structured satellite deployment mechanism with self-actuated torsion joint," *Journal of Mechanical Engineering Science and Technology (JMEST)*, vol. 8, no. 1, p. 27, Mar. 2024, doi: 10.17977/um016v8i12024p027.

[25] H. Wang, C. Fu, W. Cui, X. Zhao, and S. Qie, "Numerical simulation and experimental study on stress deformation of braided wire rope," *J Strain Anal Eng Des*, vol. 52, no. 2, pp. 69–76, Feb. 2017, doi: 10.1177/0309324716673232.

[26] T.-C. Chen, S.-T. Chen, L.-W. Tsay, and R.-K. Shiue, "Correlation between fatigue crack growth behavior and fracture surface roughness on cold-rolled austenitic stainless steels in gaseous hydrogen," *Metals (Basel)*, vol. 8, no. 4, p. 221, Mar. 2018, doi: 10.3390/met8040221.

[27] R. Prasetya, A. Andoko, and S. Suprayitno, "Camshaft failure simulation with static structural approach," *Journal of Mechanical Engineering Science and Technology*, vol. 5, no. 1, pp. 47–61, Jul. 2021, doi: 10.17977/um016v5i12021p047.

[28] R.L. Norton, *Machine Design: An Integrated Approach*, 4th ed. 2011.

[29] R. Prasetya, A. Andoko, and S. Suprayitno, "Camshaft failure simulation with static structural approach," *Journal of Mechanical Engineering Science and Technology*, vol. 5, no. 1, pp. 47–61, Jul. 2021, doi: 10.17977/um016v5i12021p047.

[30] T. Joshi, R. Sharma, V.K. Mittal, V. Gupta, and G. Krishan, "Dynamic fatigue behavior of hip joint under patient specific loadings," *International Journal of Automotive and Mechanical Engineering*, vol. 19, no. 3, pp. 10014–10027, Oct. 2022, doi: 10.15282/ijame.19.3.2022.13.0773.